Orgil *et al. Cardio-Oncology* (2025) 11:53
https://doi.org/10.1186/s40959-025-00349-y

Cardio-Oncology

RESEARCH

Open Access

Unraveling the genetic blueprint of doxorubicin-induced cardiotoxicity through systems genetics approaches

Buyan-Ochir Orgil[1,2†], Akhilesh K. Bajpai[3†], Neely Alberson[1,2], Morgan Lander[1,2], Batsaikhan Enkhzul[4], Hugo R. Martinez[5], Jeffrey A. Towbin[1,2,6], Lu Lu[3*] and Enkhsaikhan Purevjav[1,2*]

Abstract

Background Anthracycline-induced cardiotoxicity (ACT) is a significant concern for cancer survivors, while genetic basis of ACT remains unclear. This study employs a murine genetic reference population (GRP) of BXD recombinant inbred strains, derived from DBA/2J (D2) and C57BL/6J (B6) crosses, to map quantitative trait loci (QTLs) linked to doxorubicin (DOX)-induced phenotypes through systems genetics approaches.

Methods To model variability in ACT, 58 BXD strains and parental B6 and D2 mice (n ≥ 4 mice/sex/strain, 3–4-month-old) underwent an intraperitoneal injection of DOX (20 mg/kg). Survival and body weight (BW) were monitored for 10 days. Echocardiography was performed before treatment and on Day 5 post-treatment, followed by genetic mapping and Mendelian randomization analyses for identifying QTLs and candidate genes associated with DOX-induced traits and severity.

Results Parental B6 strain had 60% survival, whereas 24% of D2 mice survived on Day 10. Among BXD strains, median survival varied, with BXD77 showing the lowest at Day 4. Echocardiography revealed cardiac dysfunction and a small-heart phenotype resembling ACT patients. Significant QTLs on Chromosome 10 (86–94 Mb), Chromosome 19 (52.5–54.2 Mb) and on Chromosome 14 (103–120 Mb) were associated with the survival, mean BW loss, and left ventricular (LV) volumes and ejection fraction (EF%), respectively. MR analysis identified significant causal associations between the genes implicated in BW loss *(ADD3, HSPA12 A, SLC18 A2, PDZD8, DUSP5, CASP7*) as well as EF% and LV volumes (*GPC6, UGGT2, SLAIN1, POU4 F1, MBNL2)* in BXD mice post-DOX and heart failure outcomes in humans. Most of the top candidates showed cardiomyocyte specific expression based on scRNA-seq data.

Conclusions Survival, BW loss, and echocardiography parameters considerably varied among DOX-treated BXDs, suggesting significant influence of genetic background on expression of those traits. Several candidate genes that may modulate ACT susceptibility and heart failure were identified, providing a foundation for genetic-based risk stratification and therapeutics in cardio-oncology.

†Buyan-Ochir Orgil and Akhilesh K. Bajpai contributed equally to this work.

*Correspondence:
Lu Lu
llu@uthsc.edu
Enkhsaikhan Purevjav
epurevja@uthsc.edu
Full list of author information is available at the end of the article

Introduction

Background

Advances in cancer treatment have resulted in a five-year survival rate exceeding 85% for pediatric, adolescent, and young adult cancer patients. As a result, the number of long-term cancer survivors in the United States surpassed 19 million in 2024 [1, 2]. Nevertheless, anthracycline-induced cardiotoxicity (ACT) remains a major concern among affected survivors of childhood and adult cancers, ranking just behind cancer relapse and secondary malignancies. While early manifestations of ACT include reduction in left ventricular (LV) mass and wall thickness [3], it can present as heart failure (HF), arrhythmias, sudden cardiac death, and cardiomyopathies, with its occurrence increasing among long-term survivors [4]. Anthracyclines such as doxorubicin (DOX), daunorubicin, epirubicin, and idarubicin exert irreversible myocardial damage, leading to high mortality rates among affected patients [5–7]. The risk of HF reaches 50% in patients receiving cumulative DOX doses exceeding 500 mg/m2 [8–10]. Furthermore, exposure to anthracyclines at a young age, combined with chest-directed radiation, exacerbates cardiovascular risk across the lifespan [4, 11–13]. A key clinical challenge is the inter-individual variability in susceptibility to ACT. While some patients tolerate high anthracycline doses without systemic and cardiotoxic effects, others develop severe cardiac dysfunction even at low doses [14]. Despite rigorous studies, the susceptibility to ACT remains incompletely understood. At the same time, recent advances in cardio-oncology have led to the hypothesis that genetic variations may contribute to an individual's susceptibility to acute and chronic ACT [5, 15, 16]. This differential susceptibility underscores the need for genetic investigations to identify high-risk individuals. Genome-wide association studies (GWAS) have highlighted potential genetic contributors, yet their explanatory power remains limited due to low allele frequencies, environmental variability, and small cohort sizes. In addition, variable lifestyles, diets, other comorbidities, and the environment create more complexity in humans. Numerous animal studies are employed to understand the genetics underlying ACT vulnerability in cancer patients and survivors. However, traditional animal models rely on a single-genotype or engineered on a fixed genetic background, limiting their applicability to human genetic diversity for modelling population-based research [17].

To overcome these limitations, BXD family of recombinant inbred (RI) mice offers a powerful alternative for studying ACT susceptibility [18]. This mammalian genetic reference population (GRP) of RI mice developed by intercrossing the parental C57BL/6J (B6) and DBA/2J (D2) strains recapitulates the genetic diversity of human populations [19]. Notably, B6 parent, an "industry standard" mouse for genetic studies, has a normal heart, whereas D2 parent displays hypertrophy and fibrosis [20], making the BXD family an ideal platform for dissecting genetic predisposition to ACT [21]. Use of BXD GRPs bred and fed in laboratory conditions can point to the gene variations and genetic mechanisms because the mouse and human genomes are more than 90% syntenic. For example, using genotype, transcriptome, and sequence dataset of the BXDs, many quantitative trait loci (QTLs) and candidate genes within those significant QTLs have been cloned, including *Ubp1* for blood pressure in mouse and human [22], modifier genes, *Xirp2* and *Nos3,* in hypertrophic cardiomyopathy (HCM) [23], *Syne1* and *Myom1* modulating expression of *Mypn* in restrictive cardiomyopathy (RCM) [24], *Rpl3l* in the development of early-onset dilated cardiomyopathy (DCM) [25], and *Cyld* and *Dhx32* as a upstream regulators of *Ace2* and *Tmprss2,* through which these two transcripts interact and influence cardiac and gastrointestinal complications in COVID-19 infection [26, 27].

Understanding genetic susceptibility to ACT can inform patient stratification, preventive measures, and individualized treatment strategies in personalized medicine. This study was driven by the major hypothesis that differential susceptibility to acute ACT is associated with an individual's genetic background, including gene variations and epistatic (gene–gene) interactions. To test, we collected survival, body weight (BW) loss, and echocardiography parameters from a large GRP of BXD mice treated with DOX as the anthracycline of focus due to its widespread clinical use and its well-characterized cardiotoxic profile in both preclinical and clinical studies. Using systems genetics approaches, we then identified QTLs and candidate genes that modulate ACT-related traits and severity, and validated findings for the causal relationship with the genes for HF risks and outcomes in humans.

Methods

Mouse BXD family

QTLs responsible for 0.8 effect size of a genetic variance were detected with a power of ~0.8 using 50 BXD lines and 8~ 10 mice/strain in our previous studies [28, 29]. To determine the number of mouse strains and the *N* of mice per strain that yield detectable QTLs, power calculations were performed using R/qtlDesign [30]. Based on the results, fifty-eight BXD strains along with B6 and D2 parental lines ($n \geq 4$ mice/sex/strain, aged 3–4 months) were utilized. Mice were maintained in the 12-h light/12-h dark cycle on a standardized chow diet (6% kcal/fat, 20% protein, 74% carbohydrate). Experimental procedures were approved by the Institutional Animal Care

and Use Committee (IACUC) at the University of Tennessee Health Science Center (UTHSC).

Doxorubicin treatment and monitoring

To model ACT variability, mice received a single intraperitoneal injection of DOX (Sandoz Canada Inc) at the 20 mg/kg dosage. Survival and BW were monitored daily for 10 days. BW loss of 20% was used as the experimental endpoint. The mice were euthanized on Day 10 (Fig. 1).

Echocardiography in mice

Serial 2-dimensional transthoracic echocardiography was performed in mice at baseline (Day −1) and Day 5 post-DOX treatment. The mouse chests were treated with a chemical hair remover to reduce ultrasound attenuation one day before echocardiography. Before the test, the mice were sedated with 1% oxygenated isoflurane anesthesia, and normothermic core temperatures were maintained using a heated platform set to 37 °C. Cardiac function was then measured using B-mode, M-mode, and color Doppler with a 30-MHz transducer using Vevo2100 Micro-Imaging System (VisualSonics Inc., Toronto, Canada). Measurements of ventricular dimensions, wall thickness, and Doppler parameters, along with their analysis, were performed by two investigators who were blinded to BXD data.

Murine heart gene expression data

Gene expression data was generated from snap-frozen heart tissues collected from BXD mice aged 29 weeks, fed a chow diet, fasted overnight and euthanized under isoflurane anesthesia as described previously [29, 31]. These data were generated through our collaborative efforts at the UTHSC and are publicly accessible via GeneNetwork (http://genenetwork.org/) with accession #GN485 [EPFL/LISP BXD CD Heart Affy Mouse Gene 2.0 ST Gene Level (Jan14) RMA]. To obtain the heart gene expression, we used 58 male and female BXD strains and their parental B6 and D2 strains for microarray experiment.

Array profiling and data analysis

Briefly, RNA was extracted using the RNeasy mini kit (Qiagen, Valencia, CA, USA) according to the manufactures' protocol. The integrity and quality of the isolated RNA samples was evaluated using 2100 BioAnalyzer (Agilent Technologies) and those with RIN values > 8.0 were used for gene expression profiling using Affymetrix GeneChip Mouse Gene 1.0 ST Array at the UTHSC. Raw microarray data files were background corrected, normalized and summarized using robust multichip array (RMA) method in R software [32]. The RMA processed data was further normalized by using a modified z-score normalization, as previously described [33]. Briefly, in this method instead of setting the mean at 0 with a

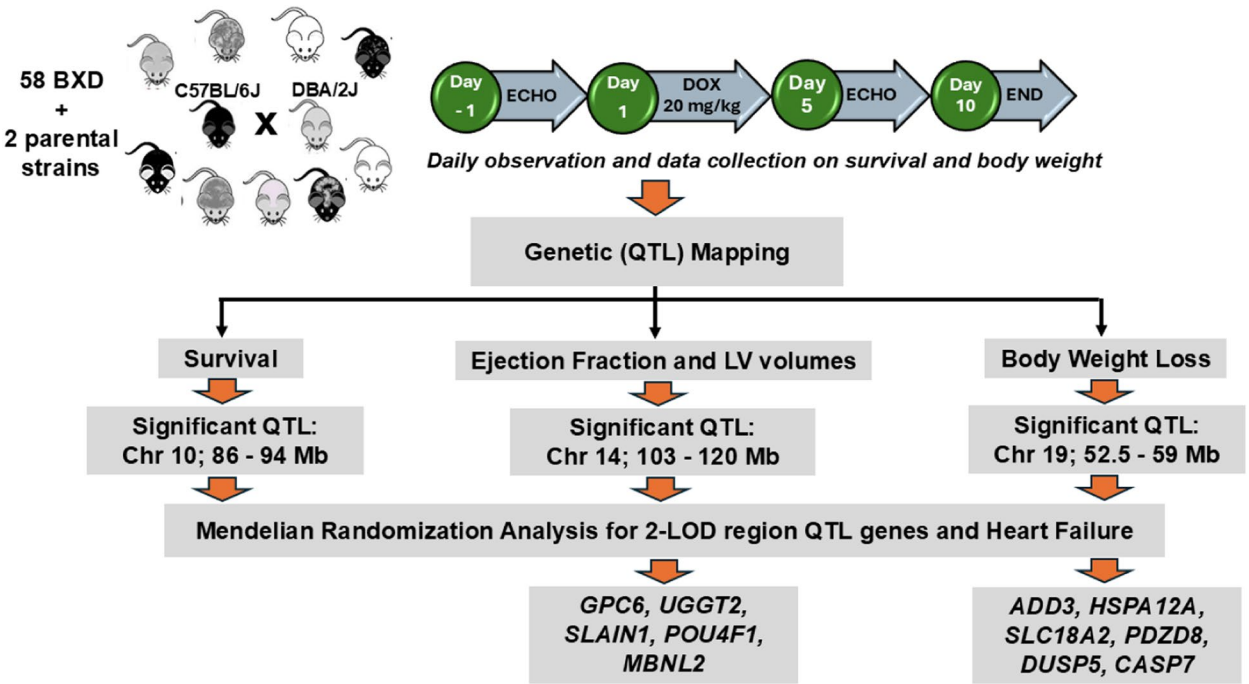

Fig. 1 Experimental scheme of phenotype collection, QTL mapping and MR analysis results in the BXD family of mice pre- and post-DOX treatment. ECHO, echocardiography; LV, left ventricular; QTL, quantitative trait locus; Chr, chromosome; LOD, logarithm of the odds

standard deviation of 1 unit, we shift up to a mean of 8 units and increase the spread by having a standard deviation of 2 units (also called as 2z +8 normalized data). This normalization removes negative values from the tables.

Generation of variant data from BXD mice

Whole-genome DNA sequencing data was generated from members of the BXD family of RI mice, as well as from the B6 and D2 parental strains. Briefly, spleens from each mouse were whole genome sequenced using the 10X Genomics Chromium platform. The raw reads in FASTQ files were aligned to the mm10/GRCm38 reference genome and VCF files were generated using the Genome Analysis ToolKit (GATK) [34]. The variant data is publicly available and can be accessed through https://www.ebi.ac.uk/ena/browser/view/PRJEB45429.

Quantitative trait loci (QTL) mapping to mouse genome

All traits (BW loss, mortality, heart mass, and cardiac function) were used for genetic mapping and analyzed using the WebQTL module on our GN website as previously described [24, 35, 36]. Likelihood ratio statistics (LRS) scores and logarithm of the odds (LOD) were computed using Haley-Knott (HK) equations [37] and GEMMA mapping method [38], respectively to evaluate the relationships between traits and specific genotype markers across murine genome. HK regression is a fast mapping method with permutation that works well with F2 intercrosses and backcrosses, while GEMMA maps with correction for kinship using a linear mixed model and can include covariates such as sex and age. The LRS and LOD scores provide a measure of the association between variation in a trait (phenotype or molecular) and genetic differences (alleles) at a particular chromosomal locus. These statistical measures are used to determine the likelihood that two loci (genes or markers) are linked. LRS is equivalent to LOD multiplied by 4.61. The LOD [39] is also roughly equivalent to the minus-log10(P). For instance, a P of 0.0001 is equivalent to an LOD of 4, which was considered by us as a significant threshold during QTL mapping. Genome-wide significance thresholds for each QTL were defined based on 10,000 to 1,000,000 permutations of trait data [40]. All analyses were performed separately and jointly for male and female mice. The candidate genes modulating DOX-induced ACT traits in QTL and eQTL regions were narrowed down using multi-criteria approach.

Candidate genes identification

We utilized a 2-LOD genetic interval to identify potential candidate genes based on their genetic, functional and causal association with heart physiology/disorders. The 2-LOD refers to the size of the genomic interval around the QTL peak. It is considered as a standard in genetic mapping, offering an optimal balance between mapping precision and detection sensitivity when identifying genomic regions linked to traits of interest. A multi-criteria system with scores ranging from 0 to 10 was employed to prioritize genes in the selected QTL region as follows: 1) The location of the variants can affect protein sequence and in most cases function. Variants, such as non-synonymous, frame shift, stop gain or loss are particularly vital. Hence, genes containing such coding variants between B6 and D2, using our previously generated whole genome sequencing (WGS) data [41] were used for further gene selection; GWAS link the variants to specific traits or diseases. 2) Hence, we obtained genes associated with cardiovascular diseases or 3) heart failure-related GWAS from the GWASCatalog database [42] and matched them with our QTL interval genes; 4) *Cis*-regulation in BXD heart, where genes located within ±5 Mb of the peak QTL were considered *cis*-regulated; 5) Differentially expressed genes (DEGs) between heart failure and control participants were used to prioritize QTL interval genes. The GEO dataset GSE120895 [43] containing HF and standard heart samples was analyzed to identify the DEGs with adjusted $P < 0.05$ and absolute fold change >1.5; 6) Expression of genes at a particular level is important for its functioning in a specific tissue. Hence, we selected genes that were found to be expressed in BXD heart with >2 TPM (transcript per million) based on RNA-seq; 7) Functional relevance in the heart based on genes collected from Mouse Genome Informatics (MGI, https://www.informatics.jax.org/) [44], International Mouse Phenotyping Consortium (IMPC, https://www.mousephenotype.org/ [45], and Rat Genome Database (RGD, https://www.rgd.mcw.edu) [46] as detailed in our previous article [25]; and 8) Mendelian Randomization (MR) analysis is a statistical method used to investigate the causal relationship between genes and diseases. Here, we performed MR test to analyze the causal relationship between the QTL genes and heart failure (HF). Genes that were found to be significantly linked to the risk of HF ($P < 0.05$) were scored. The first six criteria received a score of 1 each, whereas the last two were assigned a score of 2 each based on their overall significance. Genes with a minimum score of 30% (score 3) were then selected for further analysis.

Single cell RNA-seq (scRNA-seq) analysis

The cardiac cell-type specific expression of the top QTL genes was obtained from the Human Protein Atlas (HPA) database [47] (https://www.proteinatlas.org/). In HPA, the single cell data for heart muscle was collected from the study by Wang et al. [48] (GSE109816). The

expression data was quantified for four different human cell types (cardiomyocyte, smooth muscle cell, endothelial cell, fibroblast) represented in nine cell clusters. The raw read counts were scaled to transcripts per million protein-coding genes (pTPM) for each of the single cell clusters and then normalized (nTPM) using trimmed mean of M values (TMM) to allow comparisons between clusters. The detailed methodology for scRNA-seq data processing can be found at https://www.proteinatlas.org/about/assays+annotation#singlecell_rna.

Gene pathway analysis

To understand the biological processes and molecular mechanisms underlying ACT and to prioritize DOX-related candidate genes based on their role in critical biological processes, we performed gene pathway analysis for DEGs between untreated controls and DOX groups. The list of DEGs was uploaded to the WebGestalt website (http://www.webgestalt.org/option.php) for gene pathway analysis, which employs a hypergeometric statistical test to produce adjusted (*adj*) P values and enrichment ratios. Annotations with a minimum overlap of 5 genes and an FDR < 0.05 (Benjamini and Hochberg correction) were considered statistically significant.

Mendelian randomization (MR) analysis

We utilized 2-LOD interval genes for MR analysis to investigate the causal relationship between these genes and the risk of HF with the definition of SNPs as instrumental variables and HF datasets as outcomes. The results from this analysis were then considered for the prioritization of candidate genes. Expression QTLs (eQTLs) in heart tissues [coronary artery, heart atrial appendage, and heart left ventricle (LV)] along with their effect sizes were gathered from the GTEx Portal (https://www.gtexportal.org/home/downloads/adult-gtex/qtl) [49]. GWAS summary statistics for outcomes related to HF were sourced from the IEU OpenGWAS project [50]. The following outcomes of interest were included: ebi-a-GCST009541, ebi-a-GCST90018806, finn-b-I9_HEARTFAIL, finn-b-I9_HEARTFAIL_ALLCAUSE, finn-b-I9_HEARTFAIL_AND_ANTIHYPERT, finn-b-I9_HEARTFAIL_AND_HYPERTCARDIOM, finn-b-I9_HEARTFAIL_AND_OVERWEIGHT, finn-b-I9_HEARTFAIL_EXNONE, finn-b-I9_HEARTFAIL_NS, ukb-d-HEARTFAIL, ukb-d-I50, ukb-d-I9_HEARTFAIL, ukb-d-I9_HEARTFAIL_NS, ukb-e-428_CSA, bbj-a-109, ebi-a-GCST90018586. MR analysis was conducted using the TwoSampleMR R package [50]. We employed the inverse-variance weighted method when there was more than one eQTL, while the Wald ratio was used to assess statistical significance in single eQTL.

Statistical analysis

Data from individual mice were used to calculate the strain average, and the averaged data were then used to compare among groups. The Student's *t*-test, two-way ANOVA, or repeated-measures ANOVA over time were utilized to analyze BW and echocardiography parameters using GraphPad. At least four mice/sex from each strain were studied, and a P value < 0.05 was considered significant. Pearson's correlation analysis was used to identify relationships between baseline and post-DOX phenotypes and the expression of genes in the heart. Phenotype-correlated genes with $P < 0.05$ were selected for further studies and the DeSeq2 software was used to identify DEGs between baseline and post-DOX groups. Statistical significance was evaluated based on the *P*-value and false discovery rate (FDR). Genes with an *adjusted* $P < 0.05$ were considered significant DEGs and used for further systems genetics analysis.

Results

QTL on Chromosome 10 is significantly associated with mean survival in DOX-treated BXD strains

Varied survival and median survival rates were observed among DOX-treated BXDs (Fig. 2A). Parental B6 mice (black line) demonstrated a mean 10-day survival rate of 60%, while only 24% of D2 mice (red line) survived for 10 days after DOX treatment. Of the 58 BXD strains tested, six strains (BXD24, 45, 74, 89, 156, 177; blue dashed lines) exhibited higher survival rates than B6 controls, indicating a resilience (tolerance) to DOX. The other 52 BXD strains had a mean median survival of 6 ± 1 days, showing higher mortality rates than the B6 parent. Among those strains, 26 BXDs marked by green lines displayed lower

(See figure on next page.)

Fig. 2 The survival rates of BXD mice undergoing DOX treatment and the genetic mapping of these survival rates to the mouse genome. **A** The Kaplan–Meier curve illustrates the varying survival rates to DOX (Y-axis, %) among BXD strains. The X-axis represents days after DOX administration. Parental mice, B6 (black line) and D2 (red line), are indicated. The blue dashed lines denote BXD strains with longer survival rates than control B6 mice, while the green dashed lines represent BXD strains with shorter survival than D2 parental mice. **B** Manhattan plots display a significant 86–94 megabases (Mb) QTL on Chr10 (arrowhead) associated with survival rates from Day 6 to Day 10 in BXDs treated with DOX. The X-axis represents the chromosomal position in Mb on the mouse genome, while the Y-axis shows the peak LRS (likelihood ratio statistics) score. **C** A list of genetic variations in the top candidate genes within the Chr10 QTL identified that have genetic variations among BXD strains

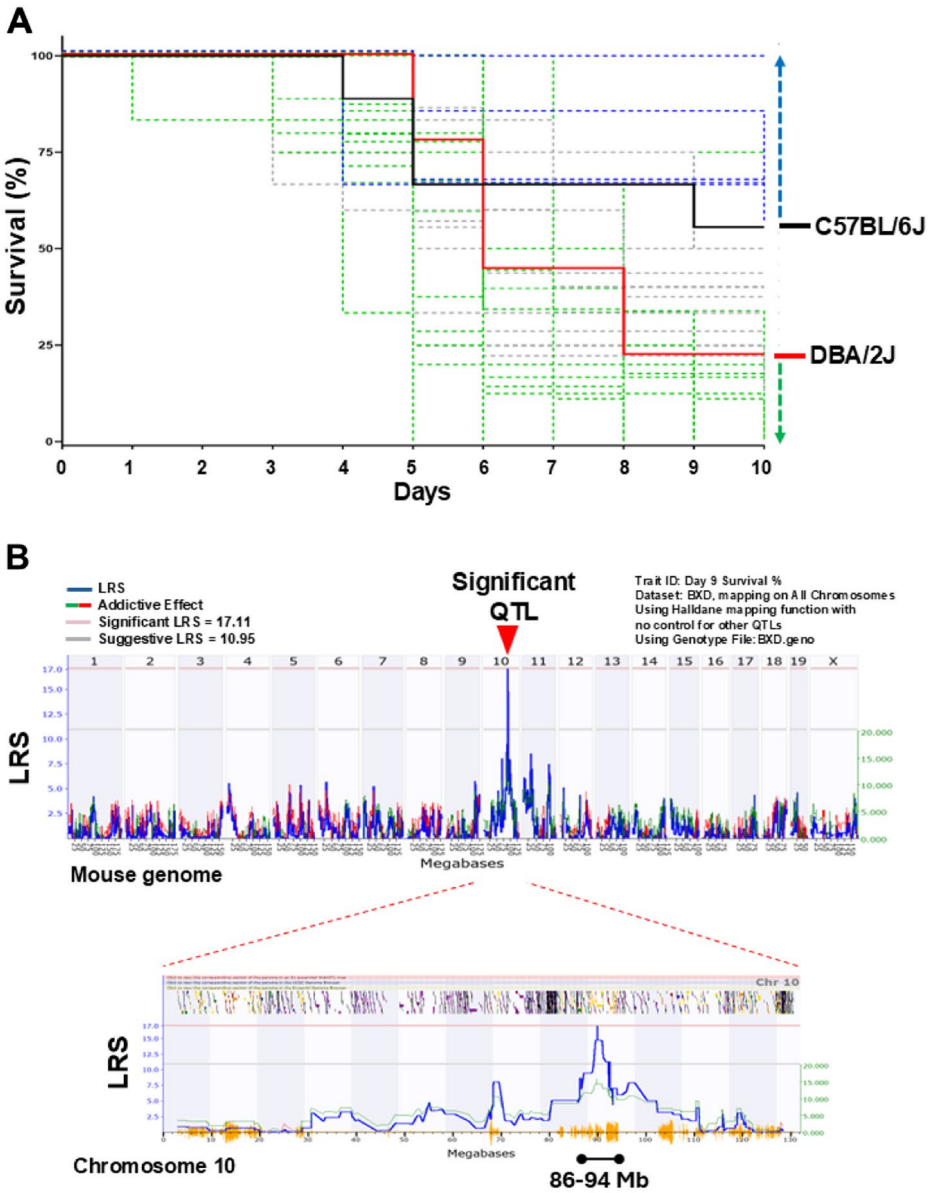

C

Chromosome	Gene variation	Symbol	Amino acid	Codons	Impact
Chr10	chr10_88419170_T/C	*Gnptab*	M/T	aTg/aCg	Moderate
Chr10	chr10_89772593_T/C	*Uhrf1bp1l*	L/P	cTa/cCa	Moderate
Chr10	chr10_91149607_C/T	*Tmpo*	V/I	Gtt/Att	Moderate
Chr10	chr10_93474948_A/G	*Lta4h*	T/A	Acc/Gcc	Moderate

Fig. 2 (See legend on previous page.)

survival rates than D2 strains. Among them, BXD77, 12, 32, 65, 75b, and 78 had the lowest median survival of 4 to 5 days, followed by BXD29, 43, 62, 69, 78, 100, 102, 113, 151, and 194 (5.4 to 6 days), suggesting that these BXDs are more susceptible (vulnerable) to DOX. Notably, the highly varied survival rates among BXDs indicated significant effects of genetic background on severity and survival traits in response to DOX. Additionally, we conducted genetic mapping to identify QTLs associated with DOX-related phenotypes observed among BXDs using the WebQTL tools available on our GN website and detected a significant QTL linked to survival rates from Day 6 to 10 among DOX-treated BXDs. This QTL is at 86–94 Mb on Chr 10 (Fig. 2B) and contains 167 genes. Notably, 15 of these genes are associated with cardiac related GWAS (Supplementary Material 1). Moreover, we refined the candidate genes within this QTL for further validation using a multi-criteria approach as described previously [31, 51], which identified *Gnptab*, *Slc25a3*, *Uhrf1bp1l,* and *Chpt1* within the Chr10 QTL as top candidate genes with a minimum 30% score. Further, genotype analysis clarified that *Gnptab* and *Uhrf1bp1l* genes had missense variants with moderate effects segregated among BXD strains (Fig. 2C).

Chromosome 19 is associated with body weight loss among DOX-treated BXD mice

Interestingly, BW loss between parental B6 (Fig. 3A, black line) and D2 (red line) mice significantly differed, reaching the maximum mean BW loss in D2 mice on D6 (14%) and BW regain was slow with only 5% increase on Day 10. In contrast, B6 mice exhibited 12% mean BW loss on Days 3–5 with sharp regain on Day 6 reaching 98% of baseline BW values on Day 10 post-DOX. The BW loss varied among BXDs following the DOX injection as well. BXD strains with significantly higher BW loss on Day 10 compared to B6 parental mice included BXD12, 154, 128, 73, and 70 (Fig. 3B). In contrast, strains BXD194 and 124 showed higher BW on Days 9–10 compared to that at the baseline, suggesting that those strains are more tolerant to DOX. Of all the 10 days tested, Day 10 revealed a significant QTL on Chr19 (52.5 ~59 Mb) associated with mean BW loss in BXDs based on both GEMMA mapping and Haley-Knott regression methods. This QTL harbored 159 genes, 19 of which were found to be significantly associated with cardiac related GWAS (Supplementary Material 1). For mean BW loss %, an overlapping QTL was identified on the same chromosome (Chr19:52.5 ~54.2 Mb) containing 40 genes. Further multi-score filtering of the genes in the larger locus identified 22 genes with a 30% score cut-off (Table 1), among which *Hspa12a, Rbm20, Adrb1,* and *Pdzd8* with a ≥ 5 significance score are considered the best candidate genes associated with mean BW loss on Day 10 post-DOX treatment (Fig. 3C-D).

DOX injection caused reduced left ventricular mass and cardiac dysfunction in BXDs

Early detection of abnormal cardiac morphology and function in cancer patients and survivors is vital to prevent residual risks of anthracycline chemotherapy for HF and cardiac death later in life [52]. Most pediatric cancer patients treated with anthracyclines who exhibit ACT have smaller hearts characterized by a shrinking myocardial and cavity size, referred to as"Grinch syndrome" [53], posing a long-term risk for cancer survivors [9]. Heart weight (HW) and HW/BW ratio measured on Day 10 revealed no significant variations of those traits among BXDs (Fig. 4A-B), suggesting concordant changes in BW and HW in mice post-DOX. However, serial echocardiography performed on Day 5 post-DOX treatment in 24 BXD lines (≥ 4 mice/sex/strain) defined abnormal small hearts with reduced left ventricular (LV) mass (Fig. 4C-D) and LV volumes at systole and diastole (Fig. 4E-F) compared to the Day −1 baseline. Notably, LV mass was significantly reduced in BXD60, 90, and 154 strains, while BXD32, 113, 154, and D2 mice showed significant reductions in LV volumes, resembling the "Grinch syndrome" observed in humans and suggesting that these strains are vulnerable to DOX (Supplemetary Material 2).

All other echocardiographic parameters, including fractional shortening (FS%), ejection fraction (EF%), heart rate (HR), and cardiac output (CO), were abnormally altered in response to DOX-treatment and varied significantly among BXDs (Fig. 5 and Supplementary Material 3). Although EF% and FS% markedly increased

(See figure on next page.)

Fig. 3 Rates of body weight (BW) loss in BXDs to DOX treatment and genetic mapping of BW loss to mouse genome. **A** Varied rates of mean BW loss in percent (%, Y-axis) among BXDs during 10 days of DOX treatment (X-axis). The BXD strains with significantly higher BW loss (green dashed lines) compared to parental D2 mice (red line) and BXDs with lower BW loss (blue dashed lines) than B6 control mice (black line) are indicated. **B** Values of BW in grams (g, Y-axis) on Day 10 post-DOX treatment among BXD mice (X-axis). Arrows indicate parental B6 and D2 mice. Asterisks (* = $P < 0.05$, ** = $P < 0.01$) indicate significant differences in BW compared with control B6 strains. **C**-**D** Manhattan plots showing a significant QTL of 52.5–59 Mb (arrowhead) on Chr19 associated with the BW loss mean in grams (g, **C**) and of 52.5–54.2 Mb in percent (%, **D**) in BXDs on Day 10. Y-axis, LRS and -logP scores

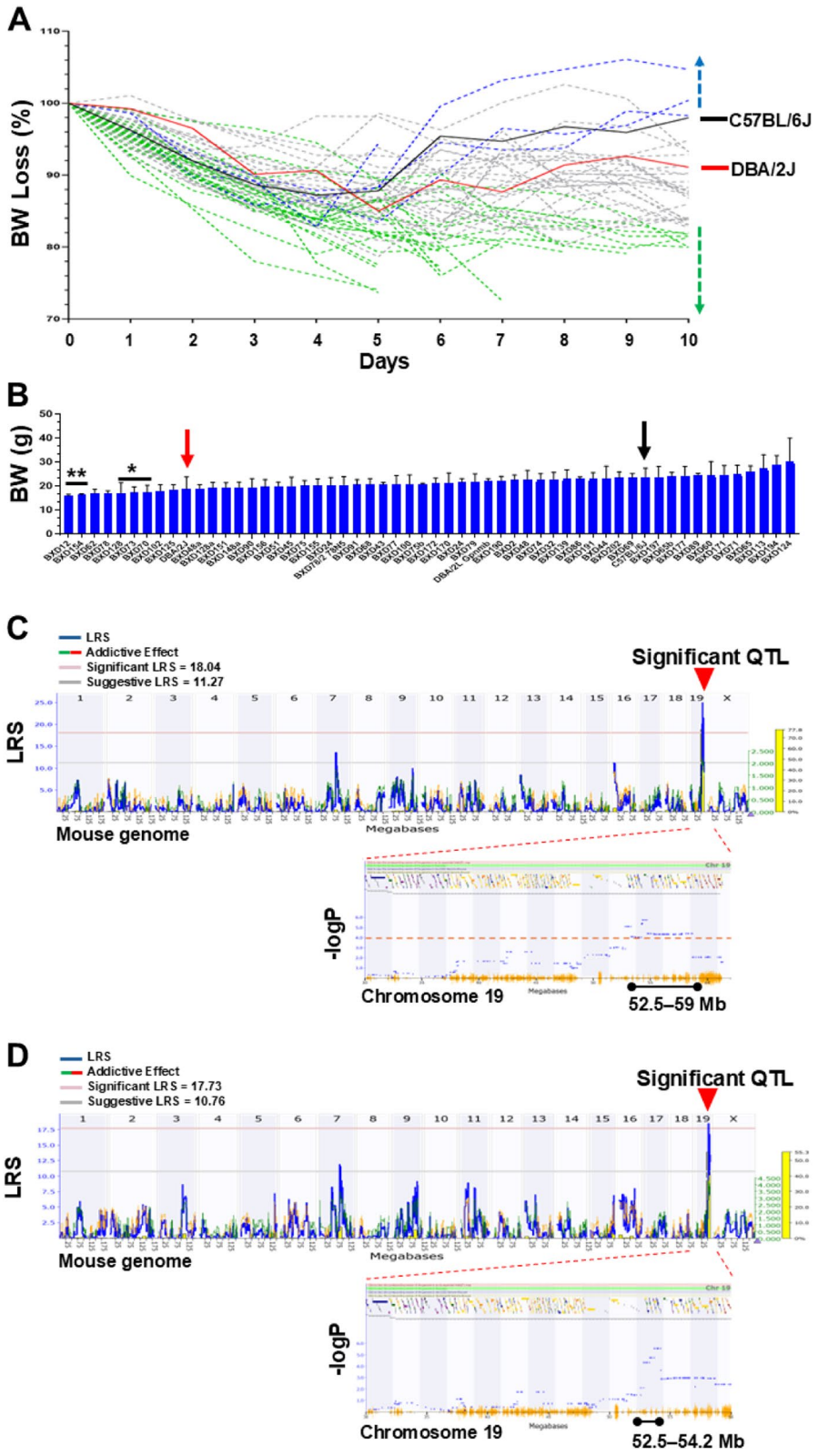

Fig. 3 (See legend on previous page.)

Table 1 List of genes with score of 30% associated with BW loss in BXDs to Day 10 of DOX treatment

Symbol	Gene Description	Coding variants between B6 and D2	GWAS (heart failure)	GWAS (cardiovascular disease)	Cis-regulation in heart	DEG in Cardiomyopathy vs Control	Functional relevance in heart	Expression in BXD heart	Mendelian Randomization	Total score
Hspa12a	heat shock protein 12A	Nonsynonymous SNP	Y	Y	Y	--	--	3.35	Y	**7**
Rbm20	RNA binding motif protein 20	Nonsynonymous SNP	--	Y	--	Y	Y	6.92	--	**6**
Adrb1	adrenergic receptor, beta 1	--	--	Y	--	Y	Y	4.32	--	**5**
Pdzd8	PDZ domain containing 8	--	--	Y	--	Y	--	3.62	Y	**5**
Pdcd4	programmed cell death 4	--	--	--	--	Y	Y	4.49	--	**4**
Shoc2	Shoc2, leucine rich repeat scaffold protein	--	--	--	--	Y	Y	3.57	--	**4**
Afap1l2	actin filament associated protein 1-like 2	missense_variant	--	Y	--	--	Y	1.86	--	**4**
Ablim1	actin-binding LIM protein 1	Nonsynonymous SNP	--	--	Y	Y	--	6.88	--	**4**
Slc18a2	solute carrier family 18 (vesicular monoamine), member 2	Nonsynonymous SNP	--	--	Y	--	--	1.26	Y	**4**
Add3	adducin 3 (gamma)	--	--	--	--	--	--	4.94	Y	**3**
Dusp5	dual specificity phosphatase 5	--	--	--	--	--	--	2.89	Y	**3**
Bbip1	BBSome interacting protein 1	--	--	--	--	--	Y	3.59	--	**3**
Adra2a	adrenergic receptor, alpha 2a	--	--	Y	--	--	Y	0.06	--	**3**
Acsl5	acyl-CoA synthetase long-chain family member 5	--	--	--	Y	--	Y	1.62	--	**3**
Vti1a	vesicle transport through interaction with t-SNAREs 1A	--	--	Y	--	Y	--	2.76	--	**3**
Tcf7l2	transcription factor 7 like 2, T cell specific, HMG box	--	Y	Y	--	--	--	3.23	--	**3**
Nrap	nebulin-related anchoring protein	Nonsynonymous SNP	--	Y	--	--	--	8.40	--	**3**
Casp7	caspase 7	--	--	--	--	--	--	3.68	Y	**3**
Nhlrc2	NHL repeat containing 2	--	--	Y	Y	--	--	3.83	--	**3**
Gfra1	glial cell line derived neurotrophic factor family receptor alpha 1	Splice site mutation	--	Y	--	--	--	2.63	--	**3**
Pnliprp2	pancreatic lipase-related protein 2	Nonsynonymous SNP	--	Y	Y	--	--	0.01	--	**3**
Rab11fip2	RAB11 family interacting protein 2 (class I)	--	--	--	Y	Y	--	2.30	--	**3**

Comment: The top candidate genes with a score of ≥ 5 out of 10 are highlighted in bold

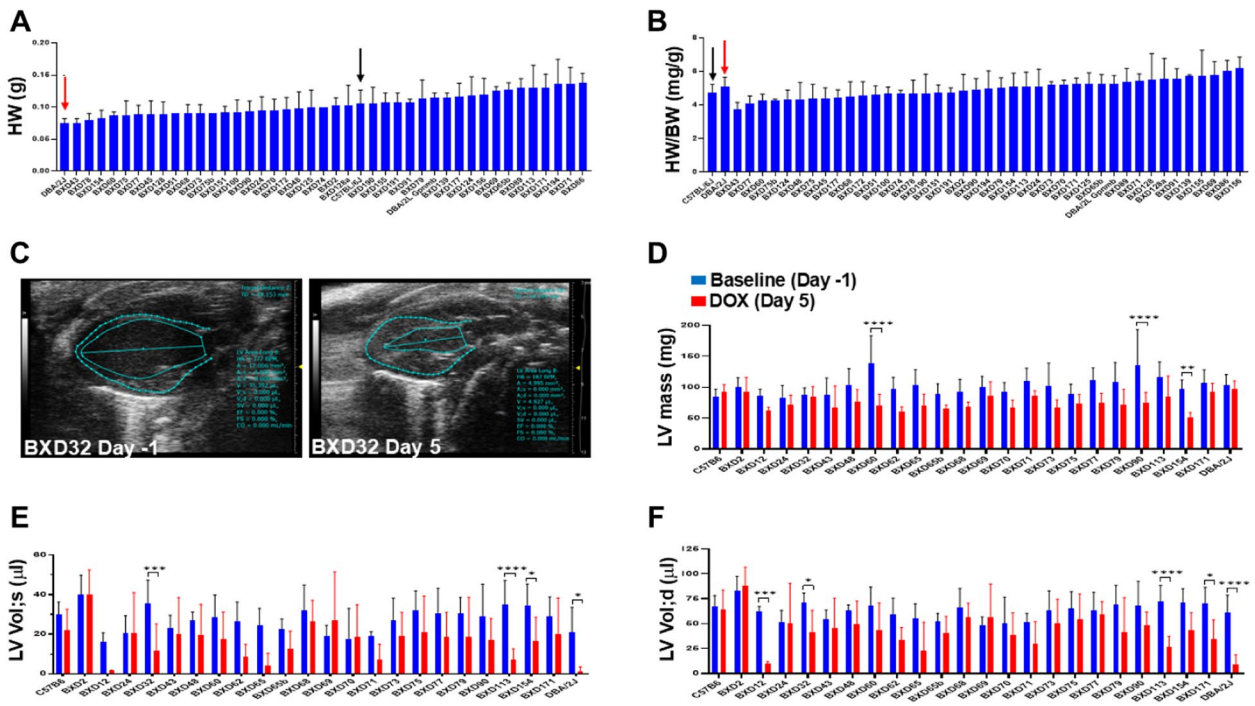

Fig. 4 Results of heart weight and echocardiographic assessment in BXDs treated with DOX. **A-B** Results of gross heart weight (HW) analysis in BXD mice on Day 10 post-DOX. Y-axis: Values of HW in grams (g, **A**) and heart weight to body weight (HW/BW, mg/g) ratio in arbitrary units (**B**) in BXD mice (X-axis). Arrows indicate parental B6 (black) and D2 (red) strains. **C** Representative echocardiographic long axis view images of BXD mouse heart at baseline (Day −1) and on Day 5 post-DOX treatment. Left ventricular (LV) walls and chamber length are indicated. **D-F** Results of comparative echocardiography assessment at the pre- and post-DOX treatment. Y-axis: Values of LV mass (mg, **D**), LV volumes (µl) at systole (s, **E**) and diastole (d, **F**) among BXDs (X-axis) at the baseline (Day −1, blue columns) compared to Day 5 post-DOX treatment (red columns). Asterisks denote significant differences (* = $P < 0.05$, ** = $P < 0.01$, *** = $P < 0.001$, **** = $P < 0.0001$) between Day −1 and Day 5

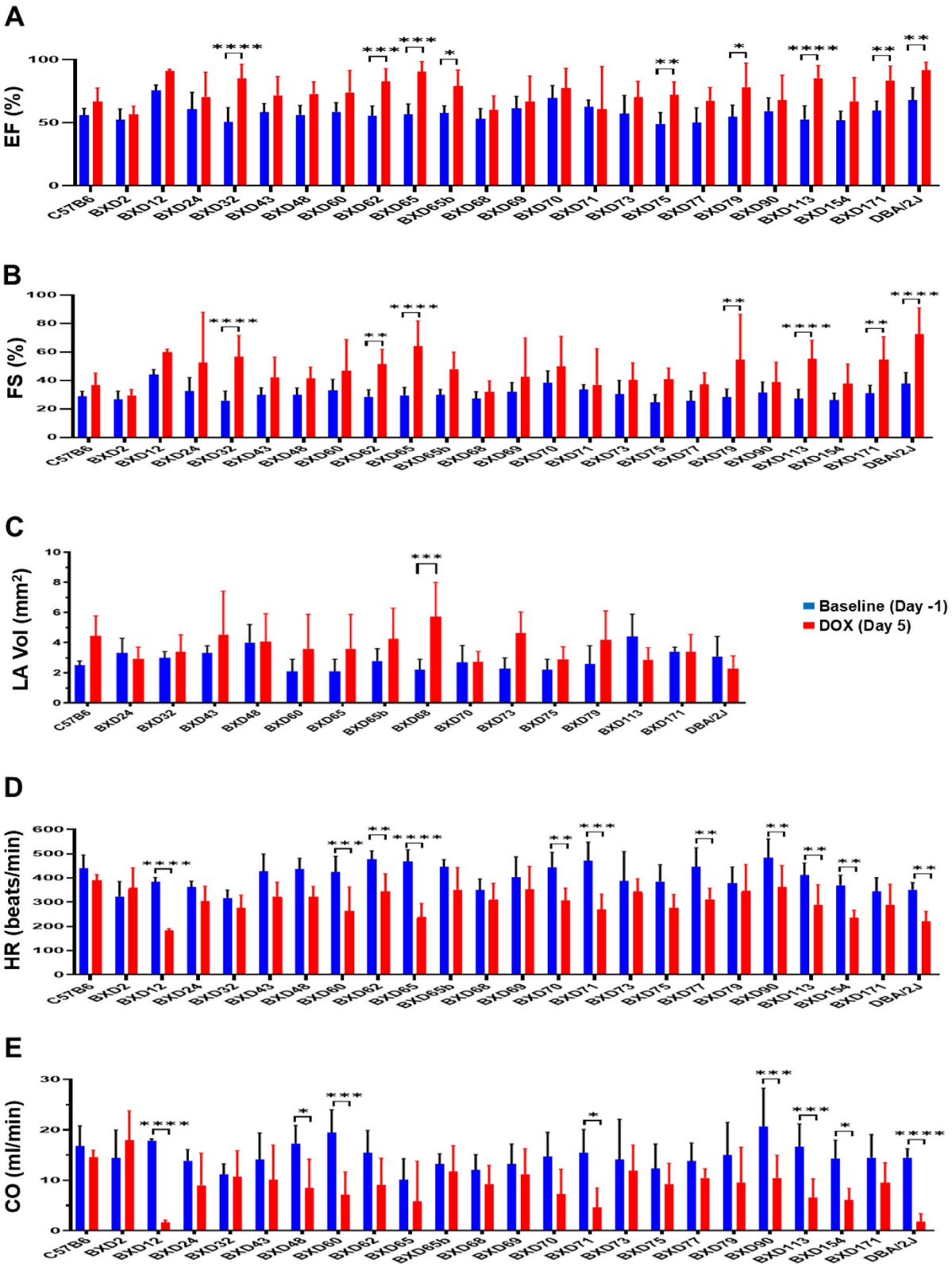

Fig. 5 Results of echocardiographic assessment of heart function in BXDs treated with DOX. Y-axis: **A**, ejection fraction (EF%); **B** fractional shortening (FS%); **C,** left atrial (LA) volumes (mm^2); **D** heart rate (HR, beats/min); **E** cardiac output (CO, ml/min) among BXDs (X-axis) at baseline (Day −1, blue columns) compared to Day 5 post-DOX treatment (red columns). Asterisks denote significant differences between Day −1 and Day 5

in many BXDs (Fig. 5A-B) presumably due to small LV volumes resulting in the increase of left atrial (LA) volume (Fig. 5C). HRs were reduced in many BXDs (Fig. 5D), resulting in CO decline post-DOX treatment, demonstrating reduction in an amount of blood pumped per minute (ml/min) by the heart to vital organs (Fig. 5E). Some BXDs (BXD12, 48, 60, 71, 90, 154) and D2 mice presented a significant decrease in CO, suggesting that these strains have greatly diminished oxygen delivery to the tissues and are more vulnerable to developing systemic toxicity and CHF. Collectively, the significantly varied traits of cardiac morphology and function among BXDs indicated the underlying impact of genetic background on the expression of all those cardiac traits in response to DOX treatment.

QTL mapping of echocardiography parameters

We conducted QTL mapping for all echocardiography parameters collected sequentially on Day −1 and Day 5 post-DOX treatment. Among the echocardiography traits, EF%, LVVol;d, and LVVol;s revealed significant QTLs on Chr14 between 103–120 Mb using GEMMA genetic mapping (Fig. 6). This QTL interval contains 211 genes, among which 9 genes were significantly associated with cardiac related GWAS. Additionally, we identified 9 genes (2 genes with cardiac related GWAS) as top candidate genes in the Chr14 QTL through our multi-score selection system (Table 2). Among those, we considered *Mycbp2*, *Abcc4* (score of 4) and *Ednrb, Gpr180, Mbnl2* with a score of 3 as strong candidate genes linked to changes in EF% and LV volumes in response to DOX due to their high levels of gene expression in BXD hearts.

Taken together, our studies in the BXD family of mice treated with DOX demonstrated varied expression of all ACT-related phenotypes (traits) tested, including survival, BW loss, cardiac function and morphology, indicating significant impacts of genetic background on these phenotypic responses to DOX treatment. We identified significant QTLs and candidate genes within the mouse genome associated ACT-related traits expressed in response to DOX, suggesting that those genes identified in murine GRP may play a role in differential susceptibility to human ACT-related phenotypes and require further causal and functional validation using MR analysis.

Cardiomyocytes display significant expression of the top candidate genes

Analysis of the top candidate genes from the three QTL regions and MR test showed high expression in cardiomyocytes in most cases (Fig. 7). Of the top four genes (*Gnptab, Slc25a3, Uhrf1bp1 l* and *Chpt1*) in the survival QTL region (Chr10: 86–94 Mb), all except *Uhrf1bp1 l*

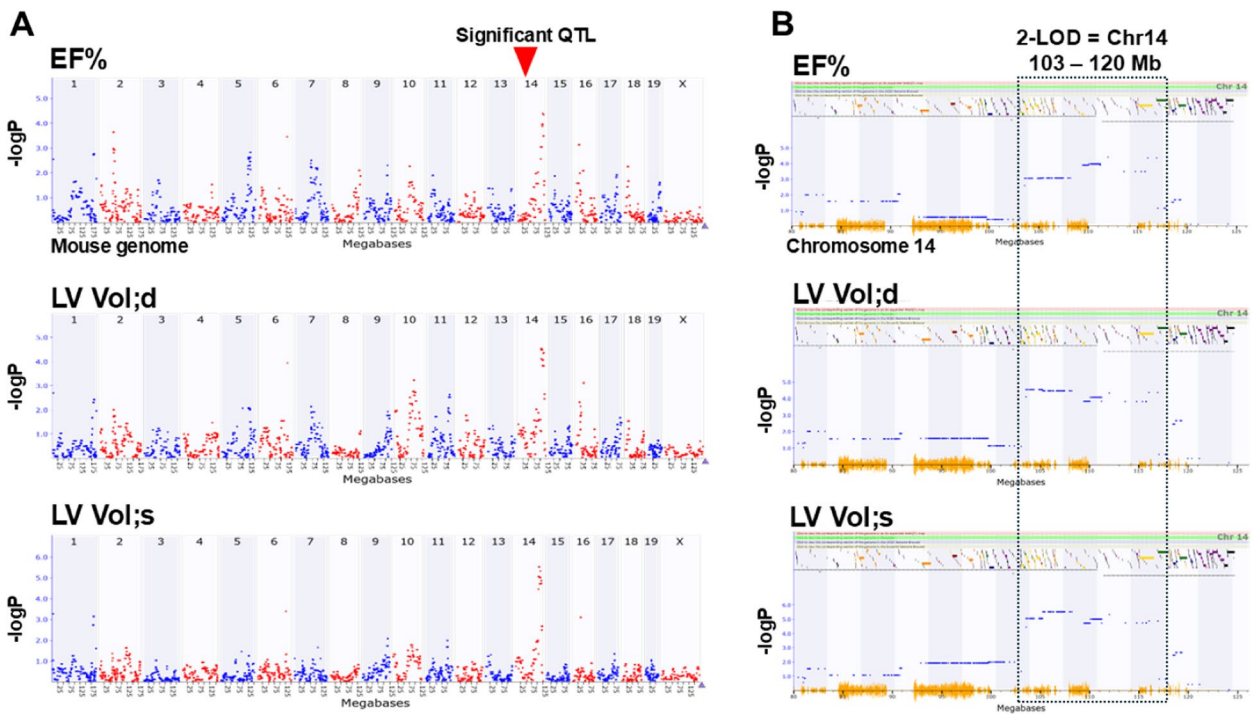

Fig. 6 Results of GEMMA genetic mapping of echocardiography traits in BXDs in response to DOX. Manhattan plots showing a significant 103–120 Mb QTL (arrowhead): (**A**) on mouse genome (X-axis); and **B** on Chr14 associated with ejection fraction (EF%) and LV volumes at systole (LV Vol;s) and diastole (LV Vol;d). Y-axis indicates an -logP score

Table 2 List of genes with a score of 30% within the Chr14 QTL associated with cardiac function traits in BXDs to DOX treatment

Symbol	Gene Description	Coding variants between B6 and D2	GWAS (heart failure)	GWAS (cardiovascular disease)	Cis-regulation in heart	DEG in Cardiomyopathy vs Control	Functional relevance in heart	Expression in BXD heart	Mendelian Randomization	Total score
Mycbp2	**MYC binding protein 2, E3 ubiquitin protein ligase**	--	--	Y	--	--	Y	2.79	--	**4**
Abcc4	**ATP-binding cassette, sub-family C (CFTR/MRP), member 4**	Nonsynonymous SNP	--	Y	--	Y	--	3.39	--	**4**
Slain1	SLAIN motif family, member 1	Nonsynonymous SNP	--	--	--	--	--	0.14	Y	**3**
Ednrb	endothelin receptor type B	Nonsynonymous SNP	--	--	--	Y	--	3.75	--	**3**
Gpc6	glypican 6	--	--	--	--	--	--	3.10	Y	**3**
Tgds	TDP-glucose 4,6-dehydratase	--	--	--	--	--	Y	2.29	--	**3**
Gpr180	G protein-coupled receptor 180	--	--	--	Y	Y	--	4.95	--	**3**
Uggt2	UDP-glucose glycoprotein glucosyltransferase 2	Nonsynonymous SNP	--	--	--	--	--	1.40	Y	**3**
Mbnl2	muscleblind like splicing factor 2	--	--	--	--	--	--	5.18	Y	**3**

Comment: The top candidate genes with a score of 4 out of 10 are highlighted in bold

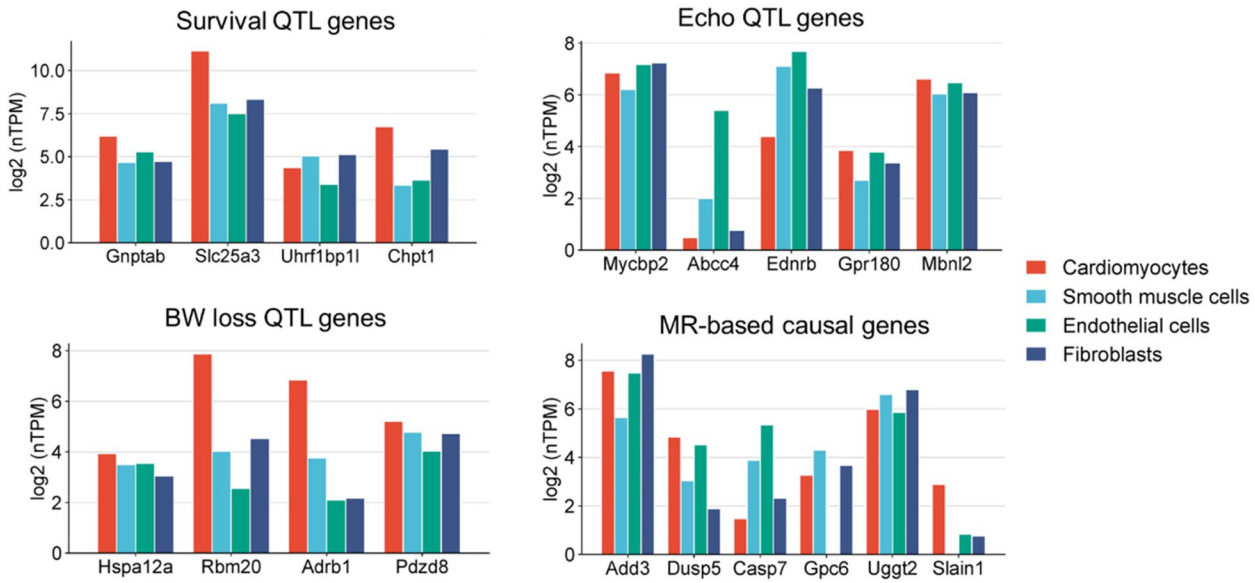

Fig. 7 Cardiac cell-type specific expression of the top candidate genes. The cell type specific expression based on single cell RNA sequencing was obtained from the Human Protein Atlas (HPA) database. The overlapping MR-test causal genes with other plots are not shown. Normalized TPM (nTPM) data corresponding to each cluster can be found in Supplementary Material 4.

showed the highest expression in cardiomyocytes with *Slc25a3* being significantly higher than the others. Similarly, all top candidates in the BW loss QTL region displayed the strongest expression in cardiomyocytes. The cell-type specific expression pattern of the top echo QTL genes was, however, different than the other two phenotypes. Among the top five candidates selected (*Mycbp2, Abcc4, Ednrb, Gpr180,* and *Mbnl2*), only *Mbnl2* displayed the strongest expression in cardiomyocytes, whereas *Abcc4* and *Ednrb* showed the strongest expression in endothelial cells. When we looked at the genes showing significant causal association based on MR test, *Dusp5* and *Slain1* showed strongest expression in cardiomyocytes, whereas *Uggt2* and *Add3* displayed strongest expression in fibroblasts. The cell-type specific expression for *Slc18a2* and *Pou4f1* could not be detected, which is consistent with the whole heart expression data. The expression of these genes in each cell cluster can be found in Supplementary Material 4.

Mendelian Randomization analysis

We used MR to analyze the causal associations between the 2-LOD interval genes and HF for both BW loss after 10 days of DOX treatment and echocardiographic traits (EF% and LV volumes). The 2-LOD interval related to BW loss post-DOX treatment contained 159 genes. We

identified 27 eQTLs corresponding to 18 genes in the heart tissues from the GTEx database. The association of these genes with sixteen HF outcomes obtained from the IEU OpenGWAS project was assessed, yielding 202 associations, and twenty of these associations, relating to 6 genes (*ADD3, HSPA12 A, SLC18 A2, PDZD8, DUSP5, CASP7*), were statistically significant with $P < 0.05$ (Table 3). Furthermore, the 2-LOD region associated with cardiac EF% and LV volumes traits included 211 genes. For 16 of these genes, 27 eQTLs in heart tissues were retrieved from the GTEx database. The association of these genes with HF outcomes resulted in a total of 234 associations, of which 14, corresponding to 5 genes (*GPC6, UGGT2, SLAIN1, POU4 F1, MBNL2*), were statistically significant (Table 4).

Discussion

Anthracycline-induced cardiotoxicity continues to be a significant cause of cardiovascular diseases and disability in cancer patients and survivors, especially among youth, the elderly, and individuals with cardiovascular comorbidities [54]. However, the clinical management of cancer patients at risk for developing ACT remains fragmented and not patient centered [55]. Early identification of genetically susceptible patients at increased risk for ACT could enable precision medicine approaches in clinics, including dose modification of anti-cancer drugs, early cardioprotective interventions, and long-term cardiac monitoring. To elucidate the genetic determinants underlying ACT risks and severity, our study utilized a systems genetics approach in the best-characterized murine GRP of BXD RI mice derived from the parental D2 strain that exhibited natural characteristics of cardiomyopathy [20, 21]. In this study, we used DOX that remains the most extensively used anthracycline and is the prototype agent in most studies investigating ACT. Our approach of testing a high dose of DOX was rationalized to facilitate robust, measurable and reproducible phenotypic differentiation for testing and selecting the most resilient lines and most vulnerable lines for system genetics methods. The study results confirmed that genetic background significantly influenced variability of ACT-related traits such as the survival, BW loss, and cardiac morphology and dysfunction phenotypes among BXD mice following DOX exposure. Notably, we observed a reduced LV mass and LV volumes in many DOX-treated BXD strains just five days post-DOX treatment, consistent with acute remodeling events that parallel with early human responses. Thus, although our modelling

Table 3 Significant causal associations between the QTL genes linked to BW loss following Day 10 post-DOX treatment and heart failure outcomes

Gene	Outcome	No. of SNPs	Method	*P* value
ADD3	Heart failure || id:ebi-a-GCST009541	1	Wald	0.01488
HSPA12 A	Heart failure || id:ebi-a-GCST009541	2	IVW	0.04871
SLC18 A2	Congestive heart failure || id:bbj-a-109	2	IVW	0.03255
SLC18 A2	Chronic heart failure || id:ebi-a-GCST90018586	2	IVW	0.00311
SLC18 A2	Chronic heart failure || id:ebi-a-GCST90018806	2	IVW	0.001679
PDZD8	Congestive heart failure || id:bbj-a-109	2	IVW	0.04751
PDZD8	Chronic heart failure || id:ebi-a-GCST90018586	2	IVW	0.004832
PDZD8	Chronic heart failure || id:ebi-a-GCST90018806	2	IVW	0.002459
DUSP5	All-cause Heart Failure || id:finn-b-I9_HEARTFAIL_ALLCAUSE	1	Wald	0.007077
DUSP5	Heart failure and antihypertensive medication || id:finn-b-I9_HEARTFAIL_AND_ANTIHYPERT	1	Wald	0.005666
DUSP5	Heart failure and bmi 25plus || id:finn-b-I9_HEARTFAIL_AND_OVERWEIGHT	1	Wald	0.007237
DUSP5	Heart failure, not strict || id:finn-b-I9_HEARTFAIL_NS	1	Wald	0.007237
DUSP5	Heart failure || id:ukb-d-HEARTFAIL	1	Wald	0.003835
DUSP5	Diagnoses—main ICD10: I50 Heart failure || id:ukb-d-I50	1	Wald	0.002606
DUSP5	Heart failure,strict || id:ukb-d-I9_HEARTFAIL	1	Wald	0.003835
DUSP5	Heart failure, not strict || id:ukb-d-I9_HEARTFAIL_NS	1	Wald	0.00383
CASP7	Congestive heart failure || id:bbj-a-109	3	IVW	0.000525
CASP7	Heart failure || id:ebi-a-GCST009541	2	IVW	0.00137
CASP7	Chronic heart failure || id:ebi-a-GCST90018586	3	IVW	7.97E-05
CASP7	Chronic heart failure || id:ebi-a-GCST90018806	3	IVW	0.00223

Comment: IVW, Inverse variance weighted

Table 4 Significant causal associations between the QTL genes linked to echocardiography EF% and LV volume traits and heart failure outcomes

Gene	Outcome	No. of SNPs	Method	*P* value
MBNL2	All-cause Heart Failure || id:finn-b-I9_HEARTFAIL_ALLCAUSE	1	Wald	0.02909
MBNL2	Heart failure and bmi 25plus || id:finn-b-I9_HEARTFAIL_AND_OVERWEIGHT	1	Wald	0.02553
MBNL2	Heart failure, not strict || id:finn-b-I9_HEARTFAIL_NS	1	Wald	0.02553
POU4 F1	Heart failure || id:ebi-a-GCST009541	1	Wald	0.009118
POU4 F1	Heart failure || id:ukb-d-HEARTFAIL	1	Wald	0.04485
POU4 F1	Diagnoses—main ICD10: I50 Heart failure || id:ukb-d-I50	1	Wald	0.04475
POU4 F1	Heart failure,strict || id:ukb-d-I9_HEARTFAIL	1	Wald	0.04485
POU4 F1	Heart failure, not strict || id:ukb-d-I9_HEARTFAIL_NS	1	Wald	0.04485
SLAIN1	Chronic heart failure || id:ebi-a-GCST90018806	1	Wald	0.04101
UGGT2	Congestive heart failure || id:bbj-a-109	3	IVW	0.04843
UGGT2	Heart failure || id:ukb-d-HEARTFAIL	3	IVW	0.02503
UGGT2	Heart failure,strict || id:ukb-d-I9_HEARTFAIL	3	IVW	0.02503
UGGT2	Heart failure, not strict || id:ukb-d-I9_HEARTFAIL_NS	3	IVW	0.02503
GPC6	Heart failure || id:ebi-a-GCST009541	2	IVW	4.48E-05

Comment: IVW, Inverse variance weighted

represents an acute exposure and carries interspecies differences paradigm, the findings directly reflect early initiating mechanisms of chronic ACT, including the so-called "Grinch syndrome" phenotype characterized by small heart size and diminished reserve capacity [9, 53]. Ultimately, time is not the driving factor—rather, it is intrinsic (perhaps genetic) susceptibility to anthracyclines toxicity that initiates and perpetuates myocardial mass loss across both the acute and chronic phases of ACT that is seen even on low to moderate doses of anthracyclines [56], suggesting that acute maladaptive mechanistic changes may lay the groundwork for progressive myocardial injury, ultimately manifesting as chronic cardiomyopathy years later.

We identified significant QTLs pinpointing important candidate genes within murine genomic regions modulating DOX-induced traits and their severity. For example, murine genes encoding proteins such as ATP-binding cassette transporter *(Abcc4)* and heat shock protein *(Hspa12a)* in the Chr19 QTL and solute carrier proteins *(Slc25a3* and *Slc18A2* on murine Chr10 and Chr19, respectively*)* have been known to be involved in cellular metabolism, mitochondrial function, epigenetic regulation, and cardiac fibrosis, aligning with findings from human studies, where specific genetic polymorphisms have been implicated in the pathogenesis of ACT [57–59]. Analysis of the scRNA-seq data displayed significant expression for most of the top candidates in cardiomyocytes including *Hspa12a* and *Slc25a3*, while a few genes, such as *Ednrb* and *Abcc4* displayed the strongest expression in endothelial cells. However, the functional significance of the cell-type specific expression of these genes in ACT toxicity warrants further investigation.

Moreover, the study identified human ACT-susceptibility genes such as *ADD3, HSPA12A, SLC18A2, PDZD8, DUSP5, CASP7, GPC6, UGGT2, SLAIN1, POU4F1, MBNL2* that were significantly associated with HF outcomes in humans (Fig. 1). Related to cancer and ACT therapeutic targets, knockdown of *PDZD8,* encoding the mitochondria-associated endoplasmic reticulum membrane protein, has been shown to significantly promote anti-tumor activity of sunitinib, an inhibitor of tyrosine kinase receptor used in combination with antioxidant pterostilbene [60], while expression of *POU4F1* (Pit-Oct-Unc domain transcription factor) significantly correlated with cancer patient survival and *POU4F1* knockdown inhibited proliferation of esophageal squamous carcinoma cells [61]. RNA-binding protein MBNL2 (muscleblind-like splicing regulator 2) has been shown to contribute to the post-transcriptional gene dysregulation in renal cell carcinoma [62], while loss-of-function mutations of *CASP7* (caspase 7) contributed to cancer pathogenesis, representing an important prognostic and therapeutic target for several solid cancers [63].

One of this study's key findings is the identification of *DUSP5* (dual specificity phosphatase 5). The DUSP5 enzyme is known to dually inactivate mitogen-activated protein kinases (MAPKs) such as extracellular signal-regulated kinases (ERK1/2) that are involved in activation of downstream targets relevant in many diseases and cancers [64]. Recent development and use of inhibitors

of ERK-signaling alone or in combination with revolutionary immune checkpoint inhibitors (ICI) targeting the receptors of cytotoxic T-lymphocyte-associated 4 (CTLA4) and programmed death-1 (PD1) proteins significantly improved survival of cancer patients [65]. However, these therapies are associated with multi-organ adverse events, including cardiotoxicity, HF, and ICI-induced myocarditis with high mortality rates of 16% to 50% in affected patients [66]. Further recent study has shown that *DUSP5* suppression supplemented with thyroid T3 hormone treatment reversed LV dilatation and dysfunction in mice with cardiac chronic DOX injury by increasing numbers of functional cardiomyocytes [67]. Based on these reports, our murine findings warranted further validation of identified genes (*DUSP5* and other) in cancer patients not only undergoing DOX treatment, but also other types of anti-cancer therapies.

While other anthracyclines (e.g., daunorubicin, epirubicin) may differ in pharmacokinetics and toxicity profiles with differing degrees and mechanisms, the successful identification of QTLs and candidate genes linked to vulnerability and resilience to DOX in BXDs provides a robust foundation to dissect shared genetic commonalities that may be conserved across this drug class. Our findings further support the potential use of genetic risk profiling to predict individual susceptibility to cardiotoxicity prior to anthracycline therapy, particularly in pediatric or high-risk cancer populations. In addition, genes identified in our study may serve as targets for cardioprotective interventions, such as pharmacogenomic-guided therapy adjustments or co-administration of protective agents in genetically vulnerable patients. Future directions include validating these gene-phenotype associations in human cohorts, integrating findings into predictive genetic screening tools, and evaluating gene-targeted interventions in preclinical models. In addition, we recognized that several genes identified within the QTLs showed strong *cis*-eQTL signals without corresponding coding changes, suggesting the contribution of non-coding regulatory regions also may play a significant role in gene regulation and disease susceptibility variation. These findings underscore the complexity of genetic regulation, in line with previous GWAS studies in cardiovascular traits, and will be identified in our future studies.

In summary, this study provides a set of genetically prioritized candidate genes potentially contributing to ACT. We suggest that future research leveraging knockout and overexpression models in mice will be essential to confirm causal roles of these genes and unravel underlying mechanisms. Additionally, corroboration in large-scale human biobanks and precision medicine initiatives will be critical for translating our murine findings into personalized risk and prediction models using systems biology approaches by integrating genetic, clinical, multi-omics (transcriptomics, proteomics, and metabolomics) data, lifestyle and environmental factors, enabling the early identification of high-risk individuals and personalized guidance in cancer patients and survivors. By bridging the gap between experimental and translational genetics and clinical risk stratification, our findings pave the way for integrative approaches to understand gene-environment interaction—such as exposing genetically susceptible strains to exercise or high-fat diets or other metabolic stressors—could illuminate how environmental or lifestyle factors influence ACT and cardioprotective therapeutic strategies, ultimately reducing the burden of cardiovascular complications in this vulnerable population.

Study limitations

Despite the strengths of our systems genetics study, several limitations must be acknowledged. First, while murine GRPs allow for controlled environmental conditions and facilitate genetic mapping, direct extrapolation to human populations with diverse environmental influences requires cautious interpretation. Therefore, genetic diversity in humans is more significant than in RI murine models bred and fed in controlled conditions, necessitating the validation of identified QTLs and candidate genes in human cohorts through GWAS or functional assays. Second, our study used high-dose acute DOX exposure to facilitate measurable phenotypic differentiation and QTL mapping. We recognize that our approach does not fully replicate the chronic, low-dose exposure typical in many cancer treatment protocols used in clinical settings. Thus, in our further preclinical studies, by incorporating repeated low-dose regimens over extended periods, we will select the most vulnerable and the most resilient BXD mice for comparing chemotherapy drugs, their dose-dependent effects, and timing of cardiac remodeling and other organs and systems damage(s). In addition, the use of a high-dose, acute DOX injury model, while facilitating robust phenotypic contrast, causes systemic toxicities—such as gastrointestinal damage—that may contribute to mortality and confound the attribution of outcomes solely to cardiac dysfunction and introduce the possibility of survival bias in functional assessments. Cardiac mechanical and functional parameters such as EF and LV volumes were measured in surviving animals up to Day 5 post-DOX from resilient BXD strains, potentially excluding data from more susceptible strains. Our future studies using chronic low-dose regimens and intermediate time points will help mitigate this bias and allow for a more complete assessment of functional decline across genetic backgrounds, gene-environment interactions over time, and delayed cardiotoxic

effects as well as to refine our understanding of the interplay between genetic background, cumulative injury, and late-onset cardiac pathology, all of which deserve independent studies. Lastly, although a Mendelian randomization analysis has been achieved for identifying causal associations between candidate genes and the risk of HF through OpenGWAS project, a functional validation of those genes is needed to confirm causal relationships between phenotypes (traits) and genetic variants and candidate gene expression through molecular biology technologies and gene targeting including CRISPR-Cas9 gene-editing and immunological methods.

Supplementary Information

The online version contains supplementary material available at https://doi.org/10.1186/s40959-025-00349-y.

Supplementary Material 1.

Supplementary Material 2.

Supplementary Material 3.

Supplementary Material 4.

Authors' contributions

BO performed all mouse experiments and phenotype data analysis and prepared this manuscript's draft. AKB performed all genotype–phenotype analyses, prepared figures, and edited the manuscript. NRA maintained animals, assisted BO in conducting experiments, and edited the manuscript. ML and EB assisted in data analysis and interpretation. JAT provided funds and edited the manuscript. HRM supervised data analysis and edited the manuscript. LL built the conception of the study, supervised gene expression analysis data of BXDs and edited the manuscript. EP acquired conception of the study, supervised all experimentation, and edited and approved the manuscript.

Funding

The study was supported in part by the National Institutes of Health R01 grants: R01 HL128350 (LL), R01 HL151438 (JAT, LL, EP).

Data availability

The expression data for heart tissues from BXD mice are available on the GeneNetwork (http://genenetwork.org/) with accession #GN485 [EPFL/LISP BXD CD Heart Affy Mouse Gene 2.0 ST Gene Level (Jan14) RMA]. All other data presented are available either in the main manuscript or in the Supplementary Material.

Declarations

Ethics approval and consent to participate

Animal studies in this study has been approved by the Institutional Animal Care and Use Committee (IACUC) at the University of Tennessee Health Science Center (UTHSC) under the protocol #21–0264 and by the Swiss cantonal veterinary authorities of Vaud under licenses 2257.0 and 2257.1.

Competing interests

The authors declare no competing interests.

Author details

[1]Department of Pediatrics, The Heart Institute, University of Tennessee Health Science Center, Memphis, TN, USA. [2]Children's Foundation Research Institute, Le Bonheur Children's Hospital, Memphis, TN, USA. [3]Department of Genetics, Genomics and Informatics, University of Tennessee Health Science Center, Memphis, TN, USA. [4]Department of Pharmacology, Toxicology and Addiction Sciences, University of Tennessee Health Science Center, Memphis, TN, USA. [5]Department of Pediatrics, Dell Medical School, The University of Texas at Austin, Austin, TX, USA. [6]Cardiology, St. Jude Children's Research Hospital, Memphis, TN, USA.

Received: 14 March 2025 Accepted: 6 May 2025
Published online: 03 June 2025

References

1. Miller KD, et al. Cancer treatment and survivorship statistics, 2022. CA Cancer J Clin. 2022;72(5):409–36.
2. DeSantis CE, et al. Cancer treatment and survivorship statistics, 2014. CA Cancer J Clin. 2014;64(4):252–71.
3. Lipshultz SE, et al. Assessment of dexrazoxane as a cardioprotectant in doxorubicin-treated children with high-risk acute lymphoblastic leukaemia: long-term follow-up of a prospective, randomised, multicentre trial. Lancet Oncol. 2010;11(10):950–61.
4. Lipshultz SE, et al. Long-term cardiovascular toxicity in children, adolescents, and young adults who receive cancer therapy: pathophysiology, course, monitoring, management, prevention, and research directions: a scientific statement from the American Heart Association. Circulation. 2013;128(17):1927–95.
5. Bhatia S. Genetics of Anthracycline Cardiomyopathy in Cancer Survivors: JACC: CardioOncology State-of-the-Art Review. JACC CardioOncol. 2020;2(4):539–52.
6. Bates JE, et al. Therapy-Related Cardiac Risk in Childhood Cancer Survivors: An Analysis of the Childhood Cancer Survivor Study. J Clin Oncol. 2019;37(13):1090–101.
7. Perez IE, et al. Cancer Therapy-Related Cardiac Dysfunction: An Overview for the Clinician. Clin Med Insights Cardiol. 2019;13:1179546819866445.
8. Carvalho FS, et al. Doxorubicin-induced cardiotoxicity: from bioenergetic failure and cell death to cardiomyopathy. Med Res Rev. 2014;34(1):106–35.
9. Favreau-Lessard AJ, Sawyer DB, Francis SA. Anthracycline Cardiomyopathy: The Plot Gets Thinner. Circ Heart Fail. 2018;11(7): e005194.
10. Singal PK, Iliskovic N. Doxorubicin-induced cardiomyopathy. N Engl J Med. 1998;339(13):900–5.
11. Stafford LK, et al. Risk of anthracycline-induced cardiac dysfunction in adolescent and young adult (AYA) cancer survivors: role of genetic susceptibility loci. Pharmacogenomics J. 2024;24(4):21.
12. Armenian SH, et al. Cardiovascular Disease in Survivors of Childhood Cancer: Insights Into Epidemiology, Pathophysiology, and Prevention. J Clin Oncol. 2018;36(21):2135–44.
13. Armenian SH, et al. Cardiovascular Disease Among Survivors of Adult-Onset Cancer: A Community-Based Retrospective Cohort Study. J Clin Oncol. 2016;34(10):1122–30.
14. Kelly MM, Sullivan MC. Differential susceptibility: an explanation for variability in life course health and developmental outcomes. ANS Adv Nurs Sci. 2023;46(3):E98–E113
15. Aminkeng F, et al. Recommendations for genetic testing to reduce the incidence of anthracycline-induced cardiotoxicity. Br J Clin Pharmacol. 2016;82(3):683–95.
16. Chow EJ, et al. New Agents, Emerging Late Effects, and the Development of Precision Survivorship. J Clin Oncol. 2018;36(21):2231–40.
17. Agoro R and Churchill GA. Challenges and opportunities for conceiving genetically diverse sickle cell mice. Trends Mol Med. 2025;31(5):413–23
18. Ashbrook DG, et al. A platform for experimental precision medicine: The extended BXD mouse family. Cell Syst. 2021;12(3):235-247 e9.
19. Taylor BA, et al. Genotyping new BXD recombinant inbred mouse strains and comparison of BXD and consensus maps. Mamm Genome. 1999;10(4):335–48.
20. Zhao W, et al. A Murine Hypertrophic Cardiomyopathy Model: The DBA/2J Strain. PLoS ONE. 2015;10(8): e0133132.
21. Orgil BO, et al. Echocardiography phenotyping in murine genetic reference population of BXD strains reveals significant eQTLs associated with cardiac function and morphology. Physiol Genomics. 2023;55(2):51–66.
22. Koutnikova H, et al. Identification of the UBP1 locus as a critical blood pressure determinant using a combination of mouse and human genetics. PLoS Genet. 2009;5(8): e1000591.
23. Chen Y, et al. Identifying modifier genes for hypertrophic cardiomyopathy. J Mol Cell Cardiol. 2020;144:119–26.

24. Gu Q, et al. Dissection of Z-disc myopalladin gene network involved in the development of restrictive cardiomyopathy using system genetics approach. World J Cardiol. 2017;9(4):320–31.
25. Bajpai AK, et al. Exploring the Regulation and Function of Rpl3l in the Development of Early-Onset Dilated Cardiomyopathy and Congestive Heart Failure Using Systems Genetics Approach. Genes (Basel). 2023;5(1):53.
26. Xu F, et al. The Genetic Dissection of Ace2 Expression Variation in the Heart of Murine Genetic Reference Population. Front Cardiovasc Med. 2020;7: 582949.
27. Xu F, et al. Ace2 and Tmprss2 Expressions Are Regulated by Dhx32 and Influence the Gastrointestinal Symptoms Caused by SARS-CoV-2. J Pers Med. 2021;11(11):1212.
28. Cook MN, et al. Identification of candidate genes that underlie the QTL on chromosome 1 that mediates genetic differences in stress-ethanol interactions. Physiol Genomics. 2015;47(8):308–17.
29. Orgil BO, et al. Echocardiography phenotyping in murine genetic reference population of BXD strains reveals significant QTLs associated with cardiac function and morphology. Physiol Genomics. 2023;55(2):51–66.
30. Sen S, et al. R/qtlDesign: inbred line cross experimental design. Mamm Genome. 2007;18(2):87–93.
31. Gu Q, et al. Systems Genetics Analysis Defines Importance Of TMEM43/LUMA For Cardiac And Metabolic Related Pathways. Physiol Genomics. 2022;54(1):22–35.
32. Bolstad BM, et al. A comparison of normalization methods for high density oligonucleotide array data based on variance and bias. Bioinformatics. 2003;19(2):185–93.
33. Chesler EJ, et al. Complex trait analysis of gene expression uncovers polygenic and pleiotropic networks that modulate nervous system function. Nat Genet. 2005;37(3):233–42.
34. DePristo MA, et al. A framework for variation discovery and genotyping using next-generation DNA sequencing data. Nat Genet. 2011;43(5):491–8.
35. Wang J, Williams RW, Manly KF. WebQTL: web-based complex trait analysis. Neuroinformatics. 2003;1(4):299–308.
36. Overall RW, et al. Genetics of the hippocampal transcriptome in mouse: a systematic survey and online neurogenomics resource. Front Neurosci. 2009;3:55.
37. Feenstra B, Skovgaard IM, Broman KW. Mapping quantitative trait loci by an extension of the Haley-Knott regression method using estimating equations. Genetics. 2006;173(4):2269–82.
38. Girolami A, et al. Study on a new chromogenic substrate for the prothrombin time determination. Folia Haematol Int Mag Klin Morphol Blutforsch. 1987;114(6):881–95.
39. Nyholt DR. All LODs are not created equal. Am J Hum Genet. 2000;67(2):282–8.
40. Churchill GA, Doerge RW. Empirical threshold values for quantitative trait mapping. Genetics. 1994;138(3):963–71.
41. Ashbrook DG, et al. Joint genetic analysis of hippocampal size in mouse and human identifies a novel gene linked to neurodegenerative disease. BMC Genomics. 2014;15:850.
42. Buniello A, et al. The NHGRI-EBI GWAS Catalog of published genome-wide association studies, targeted arrays and summary statistics 2019. Nucleic Acids Res. 2019;47(D1):D1005–12.
43. Witt E, et al. Correlation of gene expression and clinical parameters identifies a set of genes reflecting LV systolic dysfunction and morphological alterations. Physiol Genomics. 2019;51(8):356–67.
44. Smith CL, et al. Mouse Genome Database (MGD)-2018: knowledgebase for the laboratory mouse. Nucleic Acids Res. 2018;46(D1):D836–42.
45. Groza T, et al. The International Mouse Phenotyping Consortium: comprehensive knockout phenotyping underpinning the study of human disease. Nucleic Acids Res. 2023;51(D1):D1038–45.
46. Smith JR, et al. The Year of the Rat: The Rat Genome Database at 20: a multi-species knowledgebase and analysis platform. Nucleic Acids Res. 2020;48(D1):D731–42.
47. Thul PJ, Lindskog C. The human protein atlas: A spatial map of the human proteome. Protein Sci. 2018;27(1):233–44.
48. Wang L, et al. Single-cell reconstruction of the adult human heart during heart failure and recovery reveals the cellular landscape underlying cardiac function. Nat Cell Biol. 2020;22(1):108–19.
49. Consortium, G.T. The Genotype-Tissue Expression (GTEx) project. Nat Genet. 2013;45(6):580–5.
50. Hemani G, et al. The MR-Base platform supports systematic causal inference across the human phenome. Elife. 2018;7:e34408.
51. Gu Q, et al. Expression Levels of the Tnni3k Gene in the Heart Are Highly Associated with Cardiac and Glucose Metabolism-Related Phenotypes and Functional Pathways. Int J Mol Sci. 2023;24(16):12759.
52. Border WL, Effinger KE and Leger KJ, Predicting Left Ventricular Dysfunction in Childhood Cancer Survivors: In Search of the Echocardiography Holy Grail. JACC CardioOncol. 2023;5(4):486–488.
53. Lipshultz SE, et al, Hearts too small for body size after doxorubicin for childhood ALL: Grinch syndrome. J Clin Oncol. 2014;32(15_suppl):10021–10021.
54. Bansal N, et al. Strategies to prevent anthracycline-induced cardiotoxicity in cancer survivors. Cardiooncology. 2019;5:18.
55. Clark RA, et al. Cardiotoxicity after cancer treatment: a process map of the patient treatment journey. Cardiooncology. 2019;5:14.
56. Drafts BC, et al. Low to moderate dose anthracycline-based chemotherapy is associated with early noninvasive imaging evidence of subclinical cardiovascular disease. JACC Cardiovasc Imaging. 2013;6(8):877–85.
57. McDermott-Roe C, Ky B. Genetics of Anthracycline-Mediated Cardiotoxicity: Current Status and Challenges. Curr Cardiovasc Risk Rep. 2020;14(10):14.
58. Mao Q, et al. HSPA12A acts as a scaffolding protein to inhibit cardiac fibroblast activation and cardiac fibrosis. J Adv Res. 2025;67:217–29.
59. Haldrup C, et al. Large-scale evaluation of SLC18A2 in prostate cancer reveals diagnostic and prognostic biomarker potential at three molecular levels. Mol Oncol. 2016;10(6):825–37.
60. Hojo Y, et al. Sunitinib and Pterostilbene Combination Treatment Exerts Antitumor Effects in Gastric Cancer via Suppression of PDZD8. Int J Mol Sci. 2022;23(7):4002.
61. Li N, et al. Identification of POU4F1 as a novel prognostic biomarker and therapeutic target in esophageal squamous cell carcinoma. Cancer Cell Int. 2024;24(1):280.
62. Perron G, et al. A General Framework for Interrogation of mRNA Stability Programs Identifies RNA-Binding Proteins that Govern Cancer Transcriptomes. Cell Rep. 2018;23(6):1639–50.
63. Hong W, et al. Pan-cancer analysis of the CASP gene family in relation to survival, tumor-infiltrating immune cells and therapeutic targets. Genomics. 2020;112(6):4304–15.
64. Martin-Vega A and Cobb MH. Navigating the ERK1/2 MAPK Cascade. Biomolecules. 2023;13(10):1555.
65. Morante M, et al. Immune Checkpoint Inhibitors and RAS-ERK Pathway-Targeted Drugs as Combined Therapy for the Treatment of Melanoma. Biomolecules. 2022;12(11):1562.
66. Nielsen DL, et al. Immune Checkpoint Inhibitor-Induced Cardiotoxicity: A Systematic Review and Meta-Analysis. JAMA Oncol. 2024;10(10):1390–9.
67. Tan L, et al. Thyroid hormone plus dual-specificity phosphatase-5 siRNA increases the number of cardiac muscle cells and improves left ventricular contractile function in chronic doxorubicin-injured hearts. Theranostics. 2021;11(10):4790–808.

Publisher's Note